HICUM/L2 version 2.22: Release Notes

M. Schroter and A. Chakravorty

Chair for Electron Devices & Integrated Circuits (CEDIC)
University of Technology Dresden, Germany

Dept. of Electrical and Computer Engineering
University of California at San Diego, USA

mschroter@ieee.org
http://www.iee.et.tu-dresden.de/iee/eb/comp_mod.html

August 2006

Table of contents

1 Overview

HICUM/L2 version 2.21 was released in November 2005. This document describes the latest release, version 2.22, and the changes w.r.t. version 2.21 are indicated by red-colored text. This latest version 2.22 contains minor additions, bug fixes and optimizations, which are mentioned in the header of the Verilog-A code.

HICUM version 2.1 has been left unchanged for a while in order to allow (i) EDA companies to implement a stable version and (ii) users to become familiar with the model and implement an extraction infrastructure without getting confused by changes and simulator implementation issues. This strategy has turned out to work quite well and has been made possible due to the fact that (according to foundries and publications) HICUM version 2.1 is sufficiently accurate for covering existing production processes.

Over the past few years of HICUM deployment and application in circuit simulation valuable feedback has been received from users in foundries, design houses and EDA companies. Based on the gathered feedback and suggestions, priorities were defined for model improvements to be implemented in the new version 2.20 and onwards. This document contains a concise description of all changes that are required to migrate from HICUM version 2.21 to version 2.22. To get the specific changes from version 2.1 to version 2.21, please see the release notes of version 2.21. There are in total seven incompatible (temperature dependent) equations between version 2.1 and version 2.22. Efforts were made to make version 2.21 compatible with version 2.1, where three incompatible equations were detected and fixed. Presently in version 2.22, all the seven equations are fixed and further incompatibility with collector current spreading is also addressed and fixed. Note that HICUM/L2 version 2.22 behaves identically with the version 2.1 if the additional model parameters of version 2.22 are kept at their default values. The differences to version 2.1 can be divided into (a) physics-based improvements of the fundamental model equations and (b) numerical changes for improving the model implementation and runtime performance, such as reliability of convergence and computational speed. Notice though that the latter depends very much on the particular simulator, i.e. its interface and data organization, so that in various cases only recommendations for EDA vendors can be provided rather than (detailed) code. The physics-based improvements are described in detail in this release note. Also, the model description is presently being updated accordingly, also incorporating the valuable feedback from model users.

Reference code of HICUM v2.22 is available in Verilog-A. In addition, the updated model version 2.20 is already available in SPICE3F [1]. Presently, there is no release of our own simulator DEVICE [2] planned to *general* users; however, DEVICE will still be available to our direct cooperation partners and also the corresponding v2.20 and onwards. code of DEVICE will be generally available, since it contains detailed analytical derivatives compared to version 2.1.

Important note:

The model is defined by the *code implementation* rather than by the documentation, which can not be *tested* for correctness.

Acknowledgments

A number of the changes described have been suggested by and/or already implemented in various commercial simulators. In this respect, I have very much appreciated the valuable feedback and suggestions particularly from Yo-Chien Yuan, Rosana Perez and Rick Poore (Agilent), Mohamed Selim and Joel Besnard (Mentor Graphics), Thierry Burdeaux and Didier Celi (STM), Jean-Paul Malzac (Silvaco), and Adam Divergilio (Tektronix). Many thanks go also to Marek Mierzwinski (Tiburon) and Geoffrey Coram (Analog Devices) for discussions about and help with the Verilog-A implementation, to Prof. J.-C. Perraud (CAEN) for feedback regarding the prototype implementation in SPICE3F test simulations and, finally, to K.-E. Moebus and S. Komarow for their help in developing a working Verilog-A implementation and in performing thorough model testing.

The HICUM group would like to thank especially ATMEL Germany (Heilbronn), STM (Grenoble, France), IBM (Burlington, USA) and Jazz Semiconductor (Newport Beach, USA) for financial support. We also appreciate the software donations from Applied Wave Research, Cadence, Mentor Graphics and XMOD Technologies as well as wafer access from Atmel Germany, Infineon (Munich, Germany), Jazz Semiconductor, Skyworks (Newbury Park, USA), STM and TSMC (Hsinchu, Taiwan) for measurements and experimental model verification.

2 Improvements of model equations

This section describes the model improvements for each element of the equivalent circuit. Common to all elements is the temperature description, which - compared to v2.1 - has been extended both in terms of flexibility and validity range. Below, the temperature dependence of the bandgap voltage is described first.

2.1 Temperature dependent bandgap voltage

In order to allow simulations of devices fabricated in different materials and to make the model simulator-independent, a temperature dependent bandgap voltage has been added to the model equations. The formulation suggested in [3] has been selected,

$$V_g(T) = V_g(0) + K_1 T \ln(T) + K_2 T \ , \qquad (2.1.0\text{-}1)$$

the main advantages of which are

- a higher accuracy w.r.t. measured data in the relevant temperature range compared to the classical formulation, and
- compatibility with existing temperature dependent current formulations in compact models that are based on the assumption of a simple linear temperature dependence $V_g(T) = V_{g,cl}(0) - a_g T$, but higher accuracy at the same time.

Note, that in (2.1.0-1) the temperature T decreases faster towards zero than ln(T) increases towards -∞ so that the equation assumes the finite value $V_g(0)$ at T = 0. The original coefficient values are given in Table 2.1.0/1; the second row contains an improved set of parameters which is more accurate both at low temperatures and with respect to the classical formulation

$$V_g(T) = V_{g,cq}(0) - \frac{\alpha_g T^2}{T + T_g} \ . \qquad (2.1.0\text{-}2)$$

Parameter	K_1 [V/K]	K_2 [V/K]	$V_g(0)$ [V]
[3]	$-8.459\ 10^{-5}$	$3.042\ 10^{-4}$	1.1774
[4]	$-1.02377\ 10^{-4}$	$4.3215\ 10^{-4}$	1.170

Table 2.1.0/1: Coefficients for calculating the bandgap voltage in silicon as a function of temperature from (2.1.0-1). In the range from 250 to 400K, a smaller error can be obtained by simply setting $V_g(0)$=1.1777V in the original parameter set.

For compact model and application purposes, it is sometimes more convenient to re-write above equation in terms of a reference temperature T_0 (e.g. for parameter extraction), which gives

$$V_g(T) = V_g(T_0) + k_1 \frac{T}{T_0} \ln\left(\frac{T}{T_0}\right) + k_2\left(\frac{T}{T_0} - 1\right) \quad . \tag{2.1.0-3}$$

with the definitions

$$k_1 = K_1 T_0 \quad , \quad k_2 = K_2 T_0 + k_1 \ln(T_0) \quad , \tag{2.1.0-4}$$

and the bandgap voltage at the measurement reference temperature,

$$V_g(T_0) = k_2 + V_g(0) \quad . \tag{2.1.0-5}$$

Fig. 2.1.0/1 shows the temperature dependent bandgap voltage according to (2.1.0-1) compared to the most popular conventional formulations.

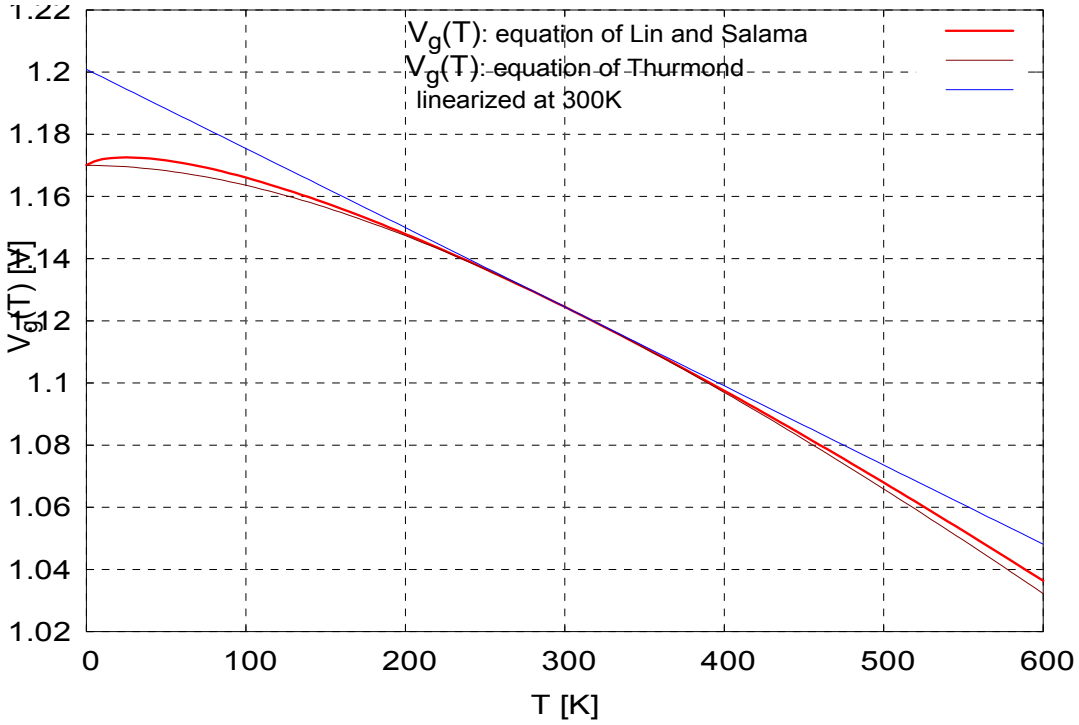

Fig. 2.1.0/1: Comparison of bandgap voltage approximations. The parameters used for (2.1.0-2) are $V_g(0) = 1.170$ V, $\alpha_g = 4.73\ 10^{-4}$ V/K, $T_g = 636$ K. The parameters for the (at T_0) linearized equation are $V_g(0) = 1.2009$ V, $a_g = 2.5461\ 10^{-4}$ V/K.

The choice of the bandgap description also influences the formulation of the effective intrinsic carrier density, which now reads

$$n_{ie}^2(T) = n_{ie}^2(T_0)\left(\frac{T}{T_0}\right)^{m_g}\exp\left[\frac{V_{geff}(0)}{V_T}\left(\frac{T}{T_0}-1\right)\right] \tag{2.1.0-6}$$

with the constant

$$m_g = 3-\frac{k_1}{V_{T0}} = 3-\frac{qK_1}{k_B}\ . \tag{2.1.0-7}$$

and K_1 from the bandgap voltage equation (2.1.0-1). Using the values in Table 2.1.0/1 for Si gives $m_g = 4.188$.

2.2 Transfer current

2.2.1 Base region reach-through

At high reverse bias across either junction, the respective space-charge region can extend throughout the whole base region (base reach-through effect). As a result, $Q_{p,T}$ in the GICCR would become zero or even less than zero which would cause numerical problems. Physically, under the reach-through condition, the current through the base is determined by thermionic emission across the base-emitter potential barrier. However, since this situation should not occur under any useful bias conditions and with physics-based model parameters, the addition of a thermionic current component does not appear to be useful from a computational and model application point of view. Such a current component and its derivatives would have to be numerically evaluated during all model calculations. Reach-through is most likely at very low current densities, where the depletion charges are small and the (always positive) minority charge is negligible. Therefore, in HICUM the hole charge at low current densities,

$$Q_{pT,j} = Q_{p0} + h_{jEi}Q_{jEi} + h_{jCi}Q_{jCi} \ , \tag{2.2.1-1}$$

is just limited to a positive value $Q_{B,rt} = 0.05Q_{p0}$, using a smoothing function, and is replaced by

$$Q_{pT,\,low} = Q_{B,\,rt}\left(1 + \frac{x + \sqrt{x^2 + a}}{2}\right) \qquad \text{with} \qquad x = \frac{Q_{pT,j}}{Q_{B,\,rt}} - 1 \tag{2.2.1-2}$$

and a = 1.921812 which reproduces the values of the former exponential smoothing function. Compared to version 2.1, only the exponential smoothing function in $Q_{pT,low}$ has now been replaced by a hyperbolic smoothing function. Also, the previous conditional statement, which turned on the evaluation of the smoothing function for $Q_{pT,j} < 0.6\ Q_{p0}$ has been removed to avoid slight inconsistencies in the calculated values and, especially, the associated derivatives.

Note, that the effect of base reach-through is extremely unlikely, so that any additional (numerical) effort to take into account the physical mechanisms occurring under these circumstances does not seem to be justified for a compact model.

2.2.2 Temperature dependence

2.2.2.1 Prefactor

In the temperature dependent expression of the model parameter c_{10} (and the associated saturation current) so far a constant value 3 has been used in the ratio $(T/T_0)^3$. Since, this factor "3" is an approximation, assuming a cancellation of the temperature dependence of the diffusivity (in a sufficiently highly doped base region), a more flexible representation is to replace "3" by the parameter ζ_{CT},

$$c_{10}(T) = c_{10}(T_0)\left(\frac{T}{T_0}\right)^{\zeta_{CT}} \exp\left[\frac{V_{gBeff}(0)}{V_T}\left(\frac{T}{T_0}-1\right)\right], \qquad (2.2.2\text{-}1)$$

with the physics-based value given by

$$\zeta_{CT} = m_g + 1 - \zeta_{\mu mB}, \qquad (2.2.2\text{-}2)$$

where $\zeta_{\mu mB}$ is the exponent factor of the mobility temperature dependence for the minority carriers in the base region. The default value is $\zeta_{CT} = 3$. The above model parameter c_{10} is shown in Fig. 2.2.2/1 as a function of temperature for various values of ζ_{CT}. Obviously, the impact of ζ_{CT} is quite small, although the selected values already cover more than the physically meaningful range.

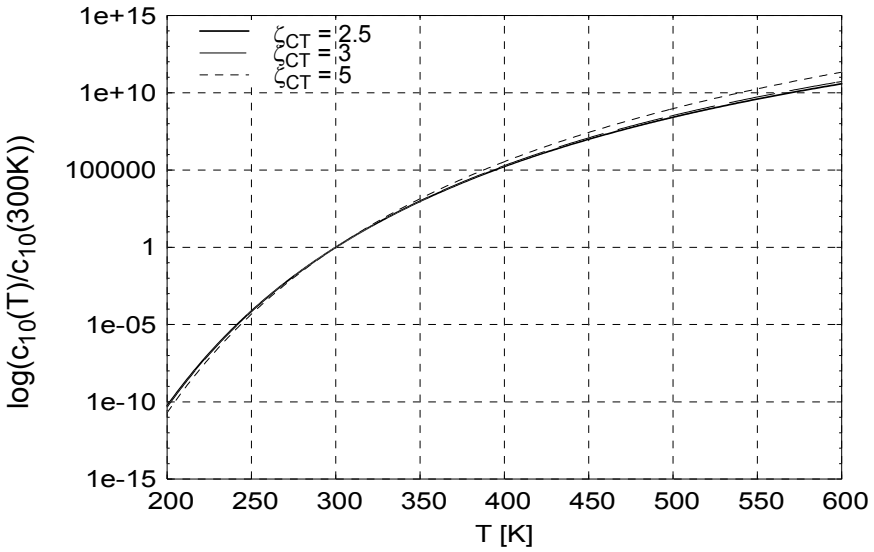

Fig. 2.2.2/1: Normalized ICCR constant vs normalized temperature with a_{CT} as parameter and fixed value of $V_{gBeff} = 1.17$V.

The background behind this change is a request for a higher flexibility in modeling the temperature dependence of the transfer current characteristic for designing bandgap-reference circuits; a more detailed study [5] has shown though, that only very large and non-physical values of ζ_{CT} do have an impact on the temperature dependent output voltage of bandgap reference circuits (in circuit simulation only, of course), and that such non-physical values of ζ_{CT} were usually accompanied with non-physical values for the bandgap voltage itself as well.

2.2.2.2 Zero-bias hole charge

Fig. 2.2.2/2 shows an example for the temperature dependence of Q_{p0}, obtained directly from 1D device simulation. The temperature dependence can be approximated by the simple expression

$$Q_{p0}(T) = Q_{p0}(T_0)\left[2 - \left(\frac{V_{DEi}(T)}{V_{DEi}(T_0)}\right)^{z_{Ei}}\right] \qquad (2.2.2\text{-}3)$$

which requires no additional model parameters. Also, the temperature derivative in the code is directly given by the already available derivative dV_{DEi}/dT. As Fig. 2.2.2/2 shows, above equation (2.2.2-3) yields excellent agreement over a large temperature range. The dependence is fairly small and does not justify the addition of a model parameter.

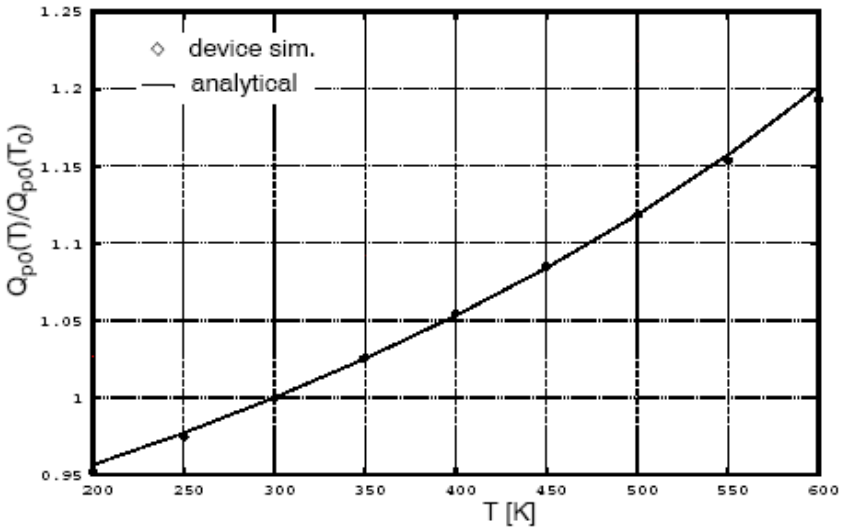

Fig. 2.2.2/2: Temperature dependence of Q_{p0} from 1D device simulation (symbols) compared to (2.2.2-3) (solid line) using existing model parameters to calculate the temperature dependence of the built-in voltage. The required internal BE depletion capacitance parameters V_{DEi} and z_{Ei} were obtained from a simple C-V fit.

2.3 Base currents

2.3.1 Excess base current from recombination at the BC barrier

In various SiGe-HBT processes, an additional base current is observable that mostly results from the additional minority charge storage in the base at the barrier caused by the Ge drop within the BC junction [7]. The typical behavior is shown in Fig. 2.3.1/1 for the base current of a SiGe-DHBT. Triggered by the collapse of the electric field in the collector at high current densities, which can be described by the critical current I_{CK}, the conduction band barrier for electrons starts to form at about V_{BE} = 0.8V for the transistor under consideration. The resulting accumulation of electrons on the base side of the BC junction is compensated by an accumulation of holes, which leads to an excess recombination rate. As a consequence, the corresponding current can be approximated to a first order by

$$i_{Bhrec} = \frac{\Delta Q_{Bf}}{\tau_{Bhrec}} , \tag{2.3.1-1}$$

with ΔQ_{Bf} as the additional minority charge in the base, which increases rapidly above I_{CK}; the corresponding recombination constant τ_{Bhrec} is a new model parameter. The current has been taken into account by adding a (controlled) current source in parallel to i_{jBEi}.

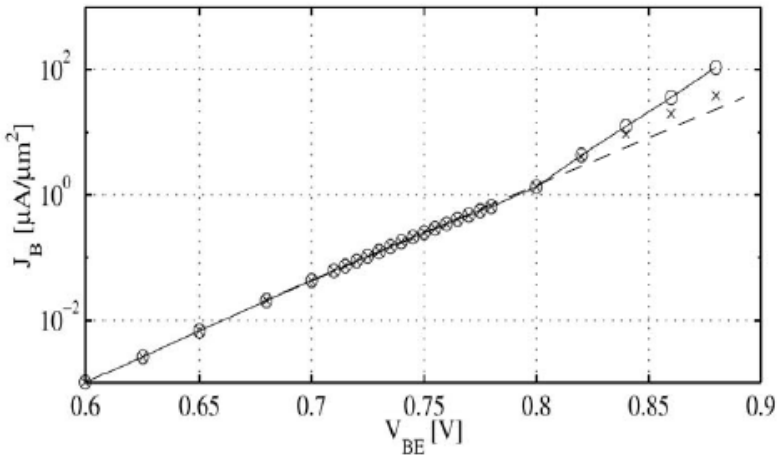

Fig. 2.3.1/1: Base current vs. base-emitter voltage for a SiGe-DHBT. Comparison between device simulation (circles), model without additional recombination component (dashed line) and model with additional recombination component (crosses).

2.3.2 Temperature dependent junction current components

The saturation current of the internal base-emitter diode is given by the following temperature dependence,

$$I_{BEiS}(T) = I_{BEiS}(T_0)\left(\frac{T}{T_0}\right)^{\zeta_{BET}} \exp\left[\frac{V_{gEeff}(0)}{V_T}\left(\frac{T}{T_0}-1\right)\right], \qquad (2.3.2\text{-}1)$$

with the new model parameters ζ_{BET} and the effective bandgap voltage $V_{gEeff}(0)$ in the emitter, which includes, e.g., high-doping effects. An estimate for $V_{gEeff}(0)$ can be calculated from the known effective bandgap voltage in the base and the measured relative TC α_{Bf} of the current gain:

$$V_{gEeff}(0) = V_{gBeff}(0) - \alpha_{Bf} T_0 \; V_{T0} \; . \qquad (2.3.2\text{-}2)$$

This estimate can be used as default or preliminary value, e.g., when converting the HICUM v2.1 parameter α_{Bf} to $V_{gEeff}(0)$. In HICUM v2.2, α_{Bf} will be phased out as a model parameter in favour of the separate model parameters ζ_{BET} and $V_{gEeff}(0)$ in an equation form that is the same for all junction components (see below). Although defining the temperature dependence of the current gain at given collector bias current is more useful for circuit design than defining a bandgap voltage from a towards $V_{B'E'} = 0$ extrapolated characteristic, the latter approach will be used in HICUM, starting from version 2.2 on in order to

- provide a more flexible description of the current gain temperature dependence,
- be consistent with the independent modeling of the bias dependence of the base current components, and
- provide a clear definition of how to extract the corresponding model parameters.

As a consequence, HICUM employs for all junction related current components, except the transfer current, equations of the form

$$I_j = I_{jS}\left[\exp\left(\frac{V}{m V_T}\right) - 1\right] \qquad (2.3.2\text{-}3)$$

with the generic temperature dependent saturation current formulation for the injection related components

$$I_{jS}(T) = I_{jS}(T_0)\left(\frac{T}{T_0}\right)^{\zeta_T}\exp\left[\frac{V_{geff}(0)}{V_T}\left(\frac{T}{T_0}-1\right)\right]. \qquad (2.3.2\text{-}4)$$

The corresponding variables that are inserted into above equation for each junction component are listed in Table 2.3.2/1. For the BE recombination components, the average value

$$V_{gBEeff} = \frac{V_{gBeff} + V_{gEeff}}{2}, \qquad (2.3.2\text{-}5)$$

that is already being used for the BE depletion capacitance components, is inserted. The temperature dependence of base-emitter recombination current components is given by n_i (rather than n_i^2 as for the injection components), the SCR width and an effective lifetime τ_{eq}. The temperature dependence of τ_{eq} and of the SCR width are very small compared to the T-dependence of n_i and also partially compensate each other. Thus, the T-dependent recombination saturation currents read:

$$I_{jRS}(T) = I_{jRS}(T_0)\left(\frac{T}{T_0}\right)^{\zeta_T/2}\exp\left[\frac{V_{geff}(0)}{2V_T}\left(\frac{T}{T_0}-1\right)\right] \qquad (2.3.2\text{-}6)$$

component I_j	V	I_S	m	V_{geff}	ζ_T
I_{jBEi}	$V_{B'E'}$	I_{BEiS}	m_{BEi}	V_{gEeff}	ζ_{BET}
I_{jBEp}	$V_{B*E'}$	I_{BEpS}	m_{BEp}	V_{gEeff}	ζ_{BET}
I_{jBCi}	$V_{B'C'}$	I_{BCiS}	m_{BCi}	V_{gCeff}	ζ_{BCiT}
I_{jBCx}	$V_{B*C'}$	I_{BCxS}	m_{BCx}	V_{gCeff}	ζ_{BCxT}
I_{jSC}	$V_{S'C'}$	I_{SCS}	m_{SC}	V_{gSeff}	ζ_{SCT}
I_{jREi}	$V_{B'E'}$	I_{REiS}	m_{REi}	V_{gBEeff}	m_g
I_{jREp}	$V_{B*E'}$	I_{REpS}	m_{REp}	V_{gBEeff}	m_g

Table 2.3.2/1: Junction current components and their corresponding parameters and controlling voltages V.

Commercially implemented SGP models contain the components I_{jBEi}, I_{jBCi} (or I_{jBCx}) and I_{jSC}. In some variants, each of these components is assigned a different set (V_{geff}, ζ_T) of parameters. Ex-

tending this to the additional components in HICUM would increase the number of parameters without significantly increasing accuracy and flexibility, or in other words: it is questionable from a practical application point of view for a compact model whether introducing separate model parameters for those base current components, that are of *little importance* for *circuit design* makes sense. Therefore, to keep the model as simple as possible (in terms of parameter determination), currents associated with same regions have been assigned the same parameters in Table 2.3.2/1. Furthermore, since the mobility exponent factor ζ_{Ci} of the internal collector region, defined by

$$\mu_{Ci}(T) = \mu_{Ci}(T_0)\left(\frac{T}{T_0}\right)^{-\zeta_{Ci}} , \tag{2.3.2-7}$$

is already available as a model parameter, the respective exponent factor for I_{jBCi} can be expressed as

$$\zeta_{BCiT} = m_g + 1 - \zeta_{Ci} . \tag{2.3.2-8}$$

with m_g from (2.1.0-7). Hence, ζ_{BCiT} does not need to be added as model parameter and is calculated internally. Similarly, the factor for the external collector current I_{jBCx} reads

$$\zeta_{BCxT} = m_g + 1 - \zeta_{Cx} \tag{2.3.2-9}$$

with the mobility factor ζ_{Cx} of the external collector (epi-)region that is also being used for modeling the temperature dependence of the minority storage time of the parasitic substrate transistor.

Since the substrate doping is fairly low, the mobility exponent factor $\zeta_{\mu pS} = 2.5$ can be assumed as a good approximation, yielding

$$\zeta_{SCT} = m_g + 1 - \zeta_{\mu pS} , \tag{2.3.2-10}$$

leaving the bandgap voltages as the only new model parameters for these regions. For silicon, the values of the above constants are: $m_g = 4.188$, $\zeta_{BCT} = 5.188-\zeta_{Ci}$, $\zeta_{SCT} = 2.69$.

2.4 Depletion capacitances and charges

In all depletion capacitance and charge formulation the exponential smoothing has been replaced by a *hyperbolic* smoothing in order to avoid numerical overflow or corresponding limiting of the argument values that are caused at large reverse voltages.

2.4.1 Bias dependence of base-emitter component

The form of the classical expressions for the internal and perimeter BE depletion charge remains the same as in the previous model version. However, the auxiliary voltage v_j has now been replaced by a *hyperbolic* smoothing expression,

$$v_j = V_f - V_T \frac{x + \sqrt{x^2 + a_{fj}}}{2} < V_f \quad . \tag{2.4.1-1}$$

using the argument

$$x = \frac{V_f - v_{B'E'}}{V_T} \quad . \tag{2.4.1-2}$$

V_f is the voltage at which at large forward bias the capacitance of the classical expression intercepts the maximum constant value [6]. In (2.4.1-1), the value of a_{fj} can be adjusted to yield results equivalent to the former formulation. If at x = 0, which corresponds to $v_{B'E'} = V_f$, the exponential and hyperbolic function values for v_j are forced to be the same, one obtains

$$a_{fj} = 4\ ln^2(2) = 1.921812 \tag{2.4.1-3}$$

which is not a model parameter, but a fixed constant within the code.

The capacitance is calculated from the derivative of the charge yielding

$$C_{jEi} = \frac{C_{jEi0}}{(1 - v_j / V_{DEi})^{z_{Ei}}} \cdot \frac{dv_j}{dv_{B'E'}} + a_{jEi} C_{jEi0} \left(1 - \frac{dv_j}{dv_{B'E'}}\right) \tag{2.4.1-4}$$

with the derivative of v_j,

$$\frac{dv_j}{dv_{B'E'}} = \frac{x + \sqrt{x^2 + a_{fj}}}{2\sqrt{x^2 + a_{fj}}} \quad . \tag{2.4.1-5}$$

Fig. 2.4.1/1 shows a comparison of the new equation with the old equation of version 2.1. There is no visible difference; the numerically calculated error is below 1.4% for $a_{jEi} = 3$, and below 1% for values of 2.4 or lower.

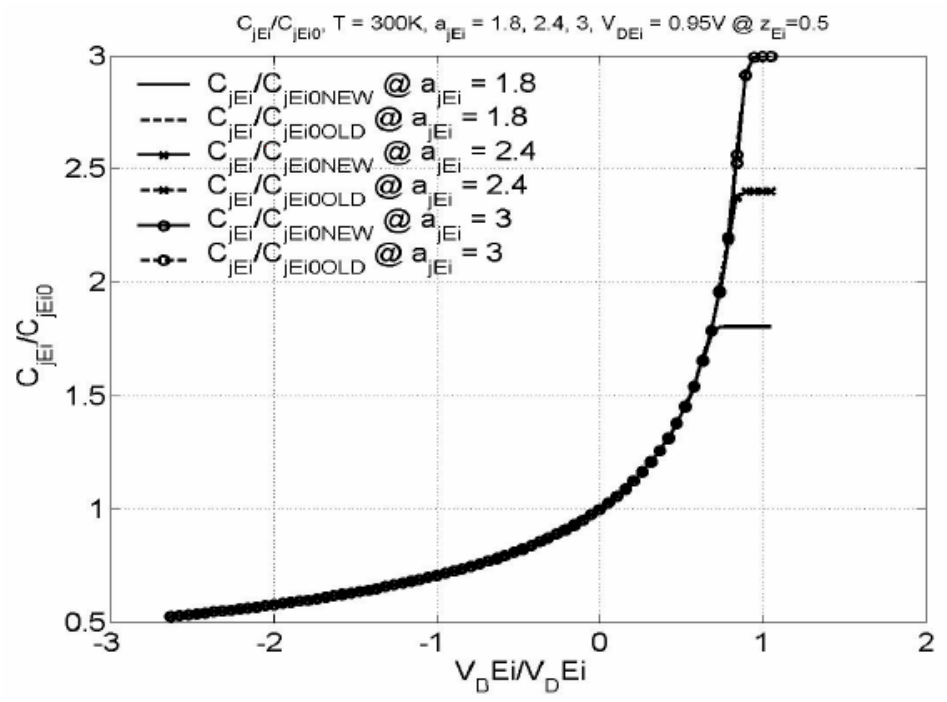

Fig. 2.4.1/1: Base-emitter depletion capacitance calculated with the new equation with a_{jEi} as parameter.

2.4.2 External depletion capacitances

The formulation for the depletion capacitances C_{jEp} also has been changed from exponential to hyperbolic smoothing functions.

2.4.3 Temperature dependence of built-in voltages

In order to avoid the built-in voltages becoming negative at high temperatures, an empirical smoothing function was included in v2.1. This function has been replaced by a physics-based formulation, that can be derived from the behavior of the intrinsic carrier density at high temperatures [8].

First, an auxiliary voltage is calculated at the reference temperature from the model parameter V_D given at the reference (or nominal) temperature T_0

$$V_{Dj}(T_0) = 2V_{T0}\ln\left[\exp\left(\frac{V_D(T_0)}{2V_{T0}}\right) - \exp\left(-\frac{V_D(T_0)}{2V_{T0}}\right)\right] \tag{2.4.3-1}$$

with the thermal voltage $V_{T0} = k_B T_0/q$. Then, the respective value at the actual temperature is calculated using the temperature dependent effective bandgap voltage of the respective junction, resulting in

$$V_{Dj}(T) = V_{Dj}(T_0)\frac{T}{T_0} - 3V_T\ln\left(\frac{T}{T_0}\right) + V_{geff}(T) - V_{geff}(T_0)\frac{T}{T_0}\ . \tag{2.4.3-2}$$

For the bandgap voltage formulation (2.1.0-1), above equation reads

$$V_{Dj}(T) = V_{Dj}(T_0)\left(\frac{T}{T_0}\right) - m_g V_T\ln\left(\frac{T}{T_0}\right) - V_{geff}(0)\left(\frac{T}{T_0} - 1\right)\ , \tag{2.4.3-3}$$

which reduces to the classical equation (that assumes a linear temperature dependence of V_{geff}) if $m_g = 3$. Finally, the new built-in voltage is calculated as

$$V_D(T) = V_{Dj}(T) + 2V_T\ln\left(\frac{1}{2}\left[1 + \sqrt{1 + 4\exp\left(-\frac{V_{Dj}(T)}{V_T}\right)}\right]\right)\ . \tag{2.4.3-4}$$

Since V_D is associated with the junction region, an average effective value is used for V_g, which is given by, e.g.,

$$V_{geff} \rightarrow V_{g(x,y)eff} = \frac{V_{gxeff} + V_{gyeff}}{2} \tag{2.4.3-5}$$

with (x,y) = (B,E), (B,C), (C,S). The temperature dependence of the built-in voltages enters the zero-bias capacitance relations. Fig. 2.4.3/1 shows the impact of the choice of the V_g value on the temperature dependence of the zero-bias capacitance.

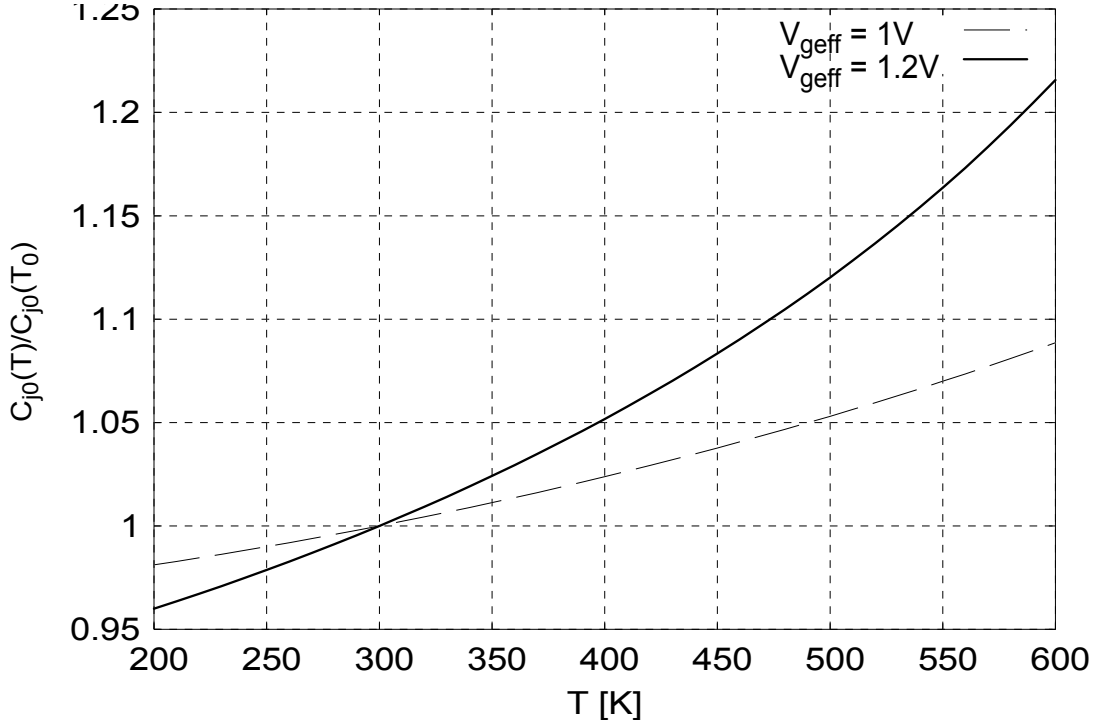

Fig. 2.4.3/1: Impact of bandgap values on the temperature dependence of the zero-bias depletion capacitance.

For electro-thermal simulations as well as for calculating the temperature coefficient of $Q_{p0}(T)$, the temperature derivative of the built-in voltage at the (parameter) reference temperature is required. In the code, the full expression for dV_D/dT as derived from (2.4.3-4) is used. However, since for $Q_{p0}(T)$ only its value at the reference (extraction) temperature T_0 is needed, the following expression can be used for parameter extraction:

$$\left.\frac{dV_D(T)}{dT}\right|_{T_0} \cong \left.\frac{dV_{Dj}(T)}{dT}\right|_{T_0} . \tag{2.4.3-6}$$

Using the expression (2.1.0-1) for the bandgap voltage gives

$$\left.\frac{dV_{Dj}(T)}{dT}\right|_{T_0} = \frac{V_{Dj}(T_0) - V_{geff}(0) - m_g V_{T0}}{T_0} . \tag{2.4.3-7}$$

As Fig. 2.4.3-1 shows, above equation is an excellent approximation for any reasonable extraction temperature.

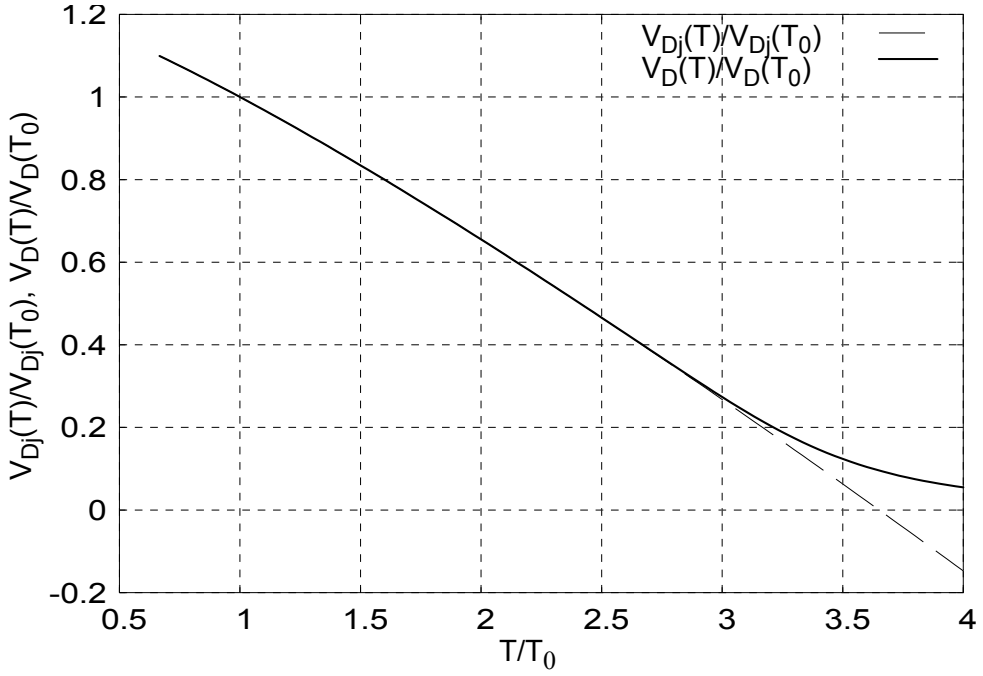

Fig. 2.4.3/2: Normalized built-in voltage vs normalized temperature (range $200 \leq T/K \leq 1200$); parameter $m_g = 3$.

2.5 Minority charge

2.5.1 Effective collector voltage and critical current

The exponential smoothing for the effective collector voltage, that is used to calculate the critical current I_{CK}, has been replaced by a *hyperbolic* smoothing to avoid arithmetic overflow for large reverse voltages $V_{B'C'}$, i.e. large values of $V_{C'E'}$. The new formulation reads

$$v_{ceff} = V_T\left[1 + \frac{u + \sqrt{u^2 + a_{vceff}}}{2}\right] \tag{2.5.1-1}$$

with the argument

$$u = \frac{v_c - V_T}{V_T} \ . \tag{2.5.1-2}$$

The value of the constant a_{vceff} (= 1.921812) has been adjusted to yield the same results as the former exponential smoothing formulation and, thus, is not a model parameter.

Furthermore, the previous numerical derivative of the critical current w.r.t. the collector potential $V_{C'}$ has been replaced by an analytical derivative. Using [6]

$$x = \frac{v_{ceff} - V_{lim}}{V_{PT}} \ , \tag{2.5.1-3}$$

the derivative is given by

$$\frac{dI_{CK}}{dV_{C'}} = \frac{dI_{CK}}{dv_{ceff}} \frac{dv_{ceff}}{dv_c} \frac{dv_c}{dV_{C'}} \ . \tag{2.5.1-4}$$

The various factors read

$$\frac{dI_{CK}}{dv_{ceff}} = \frac{I_{CK}}{v_{ceff}}\left[\frac{1}{1 + \left(\frac{v_{ceff}}{V_{lim}}\right)^2} + \frac{v_{ceff}}{V_{PT}} \frac{\frac{x + \sqrt{x^2 + a_{ickpt}}}{2}}{1 + \frac{x + \sqrt{x^2 + a_{ickpt}}}{2}} \frac{1}{\sqrt{x^2 + a_{ickpt}}}\right] \ , \tag{2.5.1-5}$$

$$\frac{dv_{ceff}}{dv_c} = \frac{dv_{ceff}}{du}\frac{du}{dv_c} = \frac{V_T}{2}\left[1 + \frac{u}{\sqrt{u^2 + a_{vceff}}}\right]\frac{1}{V_T} = \frac{u + \sqrt{u^2 + a_{vceff}}}{2\sqrt{u^2 + a_{vceff}}}\ , \tag{2.5.1-6}$$

and

$$\frac{dv_c}{dV_C} = 1\ . \tag{2.5.1-7}$$

2.5.2 Diffusion capacitances

The previous equation for the BC diffusion capacitance,

$$C_{dCi} = \tau_r S_{rc} + \tau_f S_{fc}$$

has been changed into

$$C_{dCi} = \tau_r S_{rc} \tag{2.5.2-1}$$

in order to preserve consistency between time- and frequency-domain simulation. For the same reason, the BE and BC diffusion capacitance have been extended to also include the V_C, controlled charge source

$$C_{dEi}^{C} = \tau_f S_{fc} + \left.\frac{dQ_f}{dV_{CE}}\right|_{I_{Tf},\,T}\ , \tag{2.5.2-2}$$

and the BC diffusion capacitance has been extended to include the V_B, controlled charge source

$$C_{dCi}^{B} = \tau_r S_{rb}\ . \tag{2.5.2-3}$$

2.5.3 Temperature dependence

2.5.3.1 Critical voltage V_{lim}

The voltage V_{lim} contains both collector mobility and saturation velocity,

$$V_{lim}(T) = \frac{v_s(T)}{\mu_{nCi0}(T)} \ . \tag{2.5.3-1}$$

According to [9], experimental results of the saturation velocity for T ≥ 250K can be approximated by

$$v_s(T) = v_{s0}(T_0)\left(\frac{T}{T_0}\right)^{-a_{vs}} \tag{2.5.3-2}$$

with T_0 =300K, $v_s(T_0)$ = 1.071 10^7 cm/s and a_{vs} = 0.87. The relation between a_{vs} and the existing HICUM model parameter α_{vs}, which is the relative TC, can be calculated from the derivative of (2.5.3-2) at T_0 and is given by

$$a_{vs} = \alpha_{vs} T_0 \ . \tag{2.5.3-3}$$

Inserting the temperature dependence of the collector electron mobility and (2.5.3-2) into (2.5.3-1) gives the physics-based formulation

$$V_{lim}(T) = V_{lim}(T_0)\left(\frac{T}{T_0}\right)^{\zeta_{Ci} - a_{vs}} , \tag{2.5.3-4}$$

which is simple and numerically stable, and does not require any additional model parameters. The equation is valid up to about 600K, which is the highest temperature of available experimental data for mobility and saturation velocity.

Equation (2.5.3-4) replaces the formulation used in version 2.1,

$$V_{lim}(T) = V_{lim}(T_0)(1 - \alpha_{vs}\Delta T)\left(\frac{T}{T_0}\right)^{\zeta_{Ci}} \tag{2.5.3-5}$$

where a linear temperature dependence of v_s was assumed, which could cause numerical problems in the calculation of I_{CK} for high temperatures.

2.5.3.2 Emitter transit time

The emitter time constant τ_{Ef0} depends on temperature via mainly the hole diffusivity in the neutral emitter and the current gain. Assuming a fairly large emitter concentration with a small temperature dependence of the mobility (exponent coefficient ≈0.5) the following expression can be obtained:

$$\tau_{Ef0}(T) \cong \tau_{Ef0}(T_0)\left(\frac{T}{T_0}\right)^{\zeta_{\tau Ef}} \exp\left[-\frac{\Delta V_{geff}(0)}{V_T}\left(\frac{T}{T_0}-1\right)\right] , \qquad (2.5.3\text{-}6)$$

which is also numerically stable for all temperatures. Furthermore, above equation does not require any additional model parameters, since the bandgap difference (between base and emitter region) and exponent coefficient can be calculated from already existing model parameters,

$$\Delta V_{geff}(0) = V_{gBeff}(0) - V_{gEeff}(0) , \qquad (2.5.3\text{-}7)$$

and

$$\zeta_{\tau Ef} = \zeta_{BET} - \zeta_{CT} - 0.5 . \qquad (2.5.3\text{-}8)$$

The new formulation (2.5.3-6) obviates the smoothing function in version 2.1, that was required for avoiding possible numerical problems at extreme temperatures.

2.5.4 Collector current spreading

The analytical formulation for 3D collector current spreading consists of a bias dependent portion, that has been available in version 2.1 code, and a bias independent portion that can be obtained from pre-processing the internal collector resistance in I_{CK} (e.g. using TRADICA). If the collector current spreading effect in version 2.1 is turned on by setting either one of the parameters LATB and LATL to a value greater than zero, the corresponding bias dependent equations in some cases seem to have added significant computational effort to the overall model execution time. Therefore, an alternative is proposed below, that reduces the computational effort while maintaining sufficient accuracy in the bias region of interest. The principle of the proposed solution is based on a shift of data processing from within the simulator to a preprocessing and corresponding model parameter modifications.

During the preprocessing, the complete set of 3D collector current spreading equations used so far (if LATB > 0 and/or LATL > 0) is exercised only at $I_{Tf} = I_{CK}$, resulting in the transit time $\tau_f(I_{CK})$. The latter is supposed to closely match the reference (i.e. measurements), since the transit time model parameters have been extracted from that same reference. In addition, evaluating the corresponding 1D equations with only the current spreading factor included in I_{CK} (i.e. same I_{CK} as in the 3D case), gives the (generally higher) transit time $\tau_{f,1D}(I_{CK})$. From these two time constants, a correction factor can be found,

$$f_{ccs} = \frac{\tau_f(I_{CK})}{\tau_{f,\,1D}(I_{CK})} \,, \tag{2.5.4-1}$$

which is then used to multiply the collector transit time of the 1D equations. Fig. 2.5.4/1 shows a comparison of the various curves for an extreme example with large current spreading angle (i.e. large current spreading) and a large relative contribution of the collector transit time. The corrected curves match the reference extremely well especially the region of the increase below and up to the critical current I_{CK}, and still quite well beyond I_{CK}. As a consequence, the computationally more expensive 3D current spreading calculations can be replaced in most cases, and especially for SiGe HBTs, by exercising the simpler 1D equations, in which the 3D I_{CK} values are still being used and a model parameter τ_{hcs} has been modified. The corresponding correction factor can be easily included in the modified saturation transit time:

$$\tau_{hcs} = f_{ccs}\tau_{pCs} + \tau_{Bfvs} = f_{ccs}\frac{w_C^2}{4\mu_{nC0}V_T} + \frac{w_{Bm}w_C}{2G_{\zeta i}\mu_{nC0}V_T} \ . \qquad (2.5.4\text{-}2)$$

In practice, the original model parameter τ_{hcs} will be extracted from measurements together with the partitioning factor

$$f_{thc} = \frac{\tau_{pCs}}{\tau_{hcs,x}} \ . \qquad (2.5.4\text{-}3)$$

Thus, during preprocessing for model card generation the modified extracted time constant

$$\tau_{hcs} = (1-f_{thc})\tau_{hcs,x} + f_{ccs}\tau_{pCs} = [(1-f_{thc}) + f_{ccs}f_{thc}]\tau_{hcs,x} \qquad (2.5.4\text{-}4)$$

is calculated and used as model parameter.

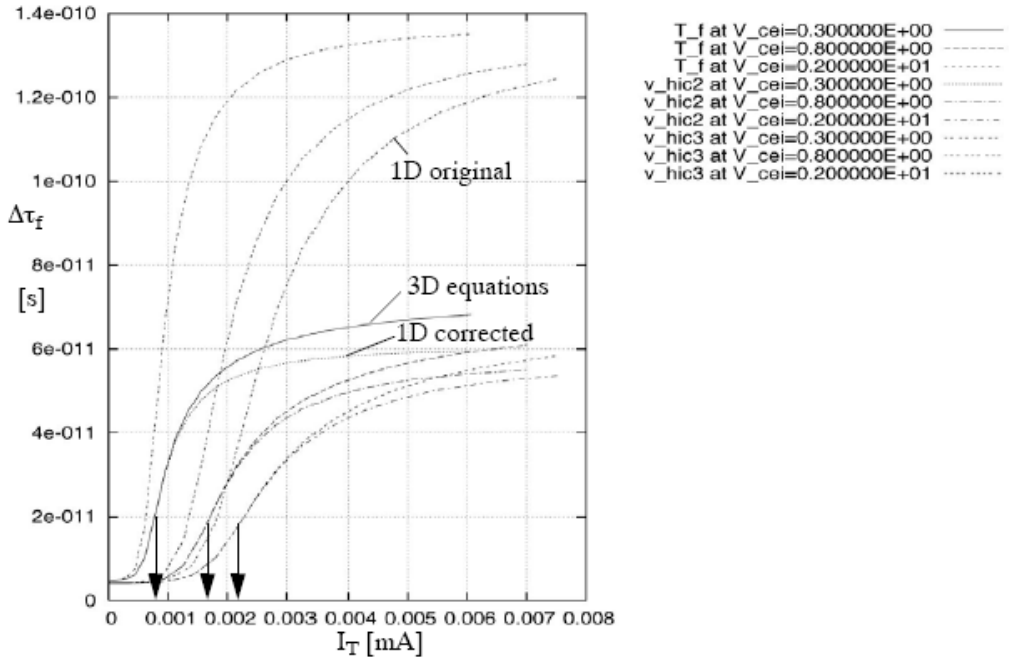

Fig. 2.5.4/1: Transit time vs. transfer current (1D test transistor) for different internal CE voltages: 3D collector current spreading equations with LTAB=5.55 and LATL=0.55 ("T_f"); 1D equations with $I_{CK}(f_{cs})$ and correction factor ("v_hic2"); the emitter transit time was turned of in this example.

2.6 Internal base resistance

Conductivity modulation is described by the expression:

$$r_i = r_{Bi0}\frac{Q_0}{Q_0 + \Delta Q_p} \tag{2.6.0-1}$$

with r_{Bi0} as zero-bias internal base resistance, and the bias dependent portion ΔQ_p of the stored hole charge,

$$\boxed{\Delta Q_p = Q_{jEi} + Q_{jCi} + Q_f + Q_r}\,. \tag{2.6.0-2}$$

Normally Q_r is negligible. Q_0 is a model parameter that is physically related and often close to the zero-bias hole charge Q_{p0}. Therefore, Q_0 is calculated from Q_{p0} as

$$\boxed{Q_0 = (1 + f_{DQr0})Q_{p0}} \tag{2.6.0-3}$$

with the factor f_{dQr0} as model parameter.

Under extreme bias conditions (such as “reach-through” with Q_{jCi} or Q_{jEi} approaching $-Q_0$) or with odd model parameters, (2.6.0-1) can cause a numerical instability due to a division by zero or a negative resistance vaue. This is avoided by ensuring that the denominator remains larger than zero under all conditions. Defining the normalized charge $q_r = 1 + \Delta Q_p / Q_0$, (2.6.0-1) is rewritten as

$$r_i = r_{Bi0}\frac{1}{f(q_r)} \quad , \tag{2.6.0-4}$$

where the smoothing function

$$f(q_r) = \frac{q_r + \sqrt{q_r^2 + a_{qr}}}{2} \quad \text{with} \quad a_{qr} = 0.01 \tag{2.6.0-5}$$

reaches the value 0.05 if q_r approaches -1. Reverse depletion charges lower than $-Q_{p0}$ ($> -Q_0$) are impossible in a real transistor. Although this is not avoided in the model, the case of a depletion

charge becoming much more negative than $-Q_0$ is extremely unlikely, but will still lead to a stable expression for r_i.

In Version 2.1, the impact of the minority charge at the emitter periphery during large-signal switching on the lumped internal base resistance was taken into account by the equation

$$r_{Bi}^{*} = r_{Bi}\frac{\Delta Q_i}{\Delta Q_p} = r_{Bi}\frac{\Delta Q_i}{\Delta Q_i + Q_{fp}} \tag{2.6.0-6}$$

with

$$\Delta Q_i = Q_{jEi} + Q_{jCi} + Q_{fi} \ . \tag{2.6.0-7}$$

For the case of a large negative BC voltage and a low forward BE voltage ($Q_f \approx 0$), $\Delta Q_i = Q_{jEi} + Q_{jCi}$ can become zero, causing a division by zero and a pole in the bias dependent r_{Bi} characteristic. Although this case is rare and is mostly likely caused by bad (non-physical) parameter combinations, it needs to be avoided under any circumstances. Therefore, to ensure numerical stability Q_{jCi} is dropped in (2.6.0-6), leading to the modified formulation of the charge difference

$$\Delta Q_i = Q_{jEi} + Q_{fi} \ , \tag{2.6.0-8}$$

which contains the change of only the major hole charge contributions w.r.t. equilibrium.

In the corresponding small-signal equation,

$$r_{Bi}^{*} = r_{Bi}\frac{C_i}{C_i + C_{dEp}} \ , \tag{2.6.0-9}$$

the internal capacitance has also to be modified to

$$C_i = C_{jEi} + C_{dEi} \ , \tag{2.6.0-10}$$

although in the small-signal case the original formulation would not cause any numerical instabilities.

From an application and accuracy point of view, dropping the BC depletion charge (and capacitance) will have only little impact, especially in those cases where r_B is of primary importance.

Another change of the formulation for the internal base resistance is that the parameter KRBI is dropped. It was introduced about 10 years ago and intended to be used for changing r_{Bi}^{*} during h.f. noise analysis due to the many uncertainties in bipolar transistor noise mechanisms and theory. With a better understanding of noise in bipolar transistors and many experimental investigations performed recently for advanced processes, this empirical parameter does not seem to be required anymore.

2.7 Base-emitter tunnelling component

2.7.1 Location of the current source

In most conventional BJT processes, the tunneling effect occurs first at the peripheral emitter junction, because the doping concentrations are highest there, and due to the curvature of that junction which leads to a narrower space-charge region and, thus, to a higher electric field. In this case, for C_e and V_e in the BE tunneling current equation [6],

$$i_{BEt} = I_{BEtS}(-V_e)C_e^{\,1-1/z_E}\exp[-a_{BEt}C_e^{\,1/z_E-1}] \quad . \tag{2.7.1-1}$$

the variables of the BE perimeter junction, i.e. C_{jEp0}, V_{DEp}, z_{Ep} and $v_{B*E'}/V_{DEp}$, respectively, have to be inserted. However, in most SiGe (and also III-V) processes, the tunnelling occurs at the internal (bottom) BE junction. In this case, C_{jEi0}, V_{DEi}, z_{Ei} and $v_{B'E'}/V_{DEi}$, respectively, need to be inserted into C_e and V_e of (2.7.1-1). Also, the tunnelling current source in the HICUM equivalent circuit needs to be connected to either the perimeter or internal base node as shown in Fig. 2.7.1/1.

Thus, in order to provide a flexible description within HICUM and, also, to also allow proper geometry scaling, a new parameter TUNODE has been introduced that defines the (base) node at which the tunneling current source is supposed to be connected. Note, that the current source has to be connected *either* to the internal base node (TUNODE = 1) *or* to the perimeter base node (TUNODE = 0), but not to both. Note, that the modification is downwards compatible.

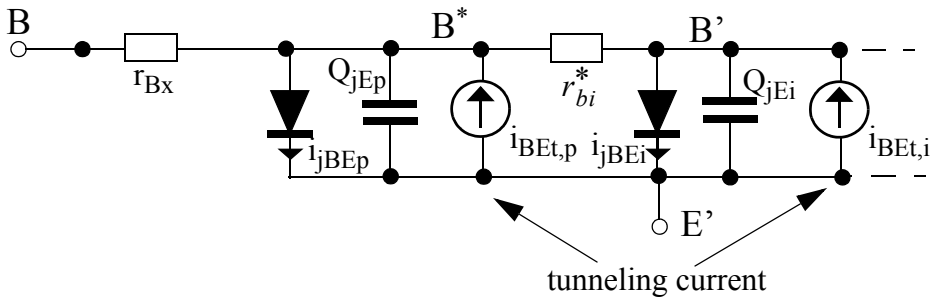

Fig. 2.7.1/1: Possible locations of the BE tunnelling current source: $i_{BEt,p}$ *or* $i_{BEt,i}$.

2.7.2 Temperature dependence

The temperature dependence of the parameters describing BE tunnelling is mainly determined by the bandgap's temperature dependence. The saturation current is given by [10]

$$I_{BEtS}(T) = I_{BEtS}(T_0)\sqrt{\frac{V_g(T_0)}{V_g(T)}}\left(\frac{V_{DE}(T)}{V_{DE}(T_0)}\right)^2\frac{C_{jE0}(T)}{C_{jE0}(T_0)} \quad , \tag{2.7.2-1}$$

while the exponent-coefficient as a function of temperature reads

$$a_{BEt}(T) = a_{BEt}(T_0)\left(\frac{V_g(T)}{V_g(T_0)}\right)^{3/2}\frac{V_{DE}(T_0)}{V_{DE}(T)}\frac{C_{jE0}(T_0)}{C_{jE0}(T)} \quad , \tag{2.7.2-2}$$

where either internal or perimeter related parameters have to be inserted for V_{DE} and C_{jE0}, according to the node assignment of the tunnelling current source. Note, that a_{BEt} now depends on temperature compared to version 2.1.

In the above equations, no additional model parameters are required since the model internal band-gap voltage (cf. eq. (2.1.0-1)) can be used in contrast to version 2.1, in which a simplified calculation was employed or the simulator bandgap voltage was used. Employing the model internal band-gap voltage also enables the evaluation of the above parameters for different materials. Since the tunneling current is associated with the BE junction region, physically the bandgap voltage corresponds to the average value of the base and emitter bandgap voltage,

$$V_g(T) = V_{gBEeff}(T) = \frac{V_{gBeff}(T) + V_{gEeff}(T)}{2}, \qquad (2.7.2\text{-}3)$$

which is already available from the calculation of the BE depletion capacitance and junction saturation current component. However, only the ratio of the bandgap voltages enters the equations (2.7.2-1) and (2.7.2-2).

Fig. 2.7.2/1 shows an example for the temperature dependence of the model parameters calculated from (2.7.2-1) and (2.7.2-2).

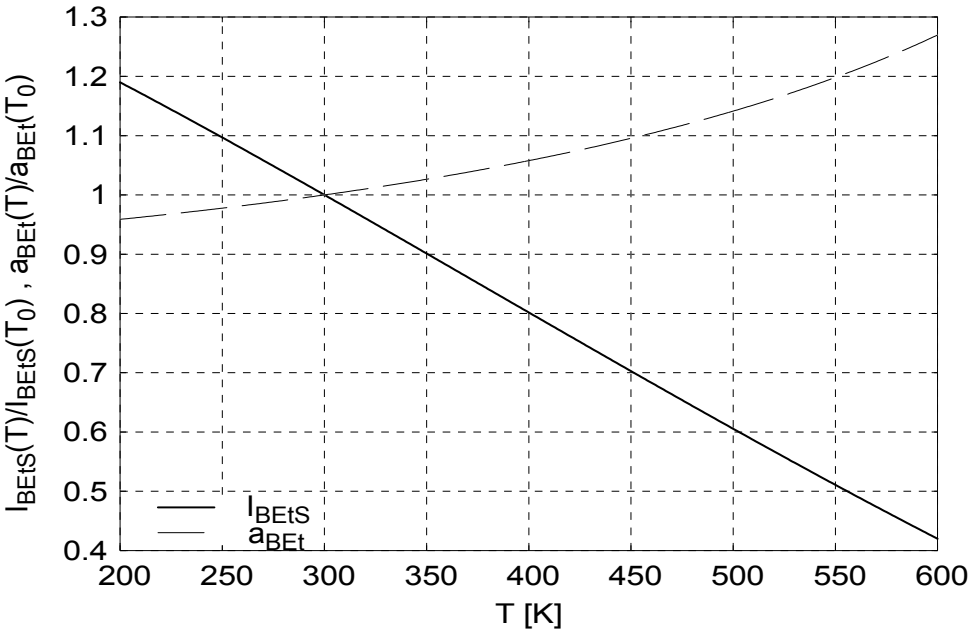

Fig. 2.7.2/1: Example for the temperature dependence of tunnelling current parameters, normalized to their values at 300K.

2.8 Parasitic base-emitter capacitance partitioning

Physically, the BE isolation capacitance C_{Eox}, which is caused by the base-emitter spacer region, and the external base resistance have a distributed character, as shown in Fig. 2.8.0/1(a). Moreover, in advanced processes, the isolation capacitance increases due to a smaller spacer thickness, while the base-emitter perimeter junction capacitance C_{jEp}, represented by its charge element charge Q_{jEp} in Fig. 2.8.0/1(b), is decreasing due to shallower emitter junction depths. The exact representation of these elements in a compact model for an accurate high-frequency description depends on the contributions of the various base resistance and capacitance portions and the geometry of the BE spacer isolation region. In addition to the BE spacer related capacitance C_{Eox}, the parasitic capacitance $C_{BE,metal}$ (and its associated charge $Q_{BE,metal}$) from the metal contact studs on top of the base and emitter poly-silicon increases with shrinking design rules. This capacitance, which belongs to the layout (p-cell) and thus to the transistor model, is connected directly between the base and emitter terminals.

For a compact model, a lumped representation of both the external base resistance and the parasitic capacitances is required. For this, a π-equivalent circuit is the best first-order compromise (cf. Fig. 2.8.0/1(b)) that allows an improved high-frequency modeling. Therefore, the distributed isolation capacitance is partitioned between the perimeter and external base node to make the model more flexible for a larger variety of processes. For instance, if the resistance contribution of the spacer region to the total external base resistance dominates, most of C_{Eox} needs to be assigned to to the internal base node ($C_{Eox,2}$). The partitioning of C_{Eox} in form of a π-equivalent circuit also allows to include the metal capacitance without any additional effort.

The partitioning option requires as model parameters the specification of either the partial capacitance components at each node or the total parasitic BE capacitance,

$$C_{BEpar} = C_{Eox} + C_{BE,metal} \,, \tag{2.8.0-1}$$

and a partitioning factor. The latter option is more convenient from a user's point of view and, hence, employed in HICUM. The respective model parameter

$$f_{BEpar} = \frac{C_{BEpar,2}}{C_{BEpar}} = \frac{C_{Eox,2} + C_{BE,metal}}{C_{Eox} + C_{BE,metal}} \tag{2.8.0-2}$$

is defined as the ratio of the "inner" to the total (measured) parasitic capacitance. Thus, the value $f_{BEpar} = 0$ indicates that the whole parasitic capacitance is connected between the transistor terminals.

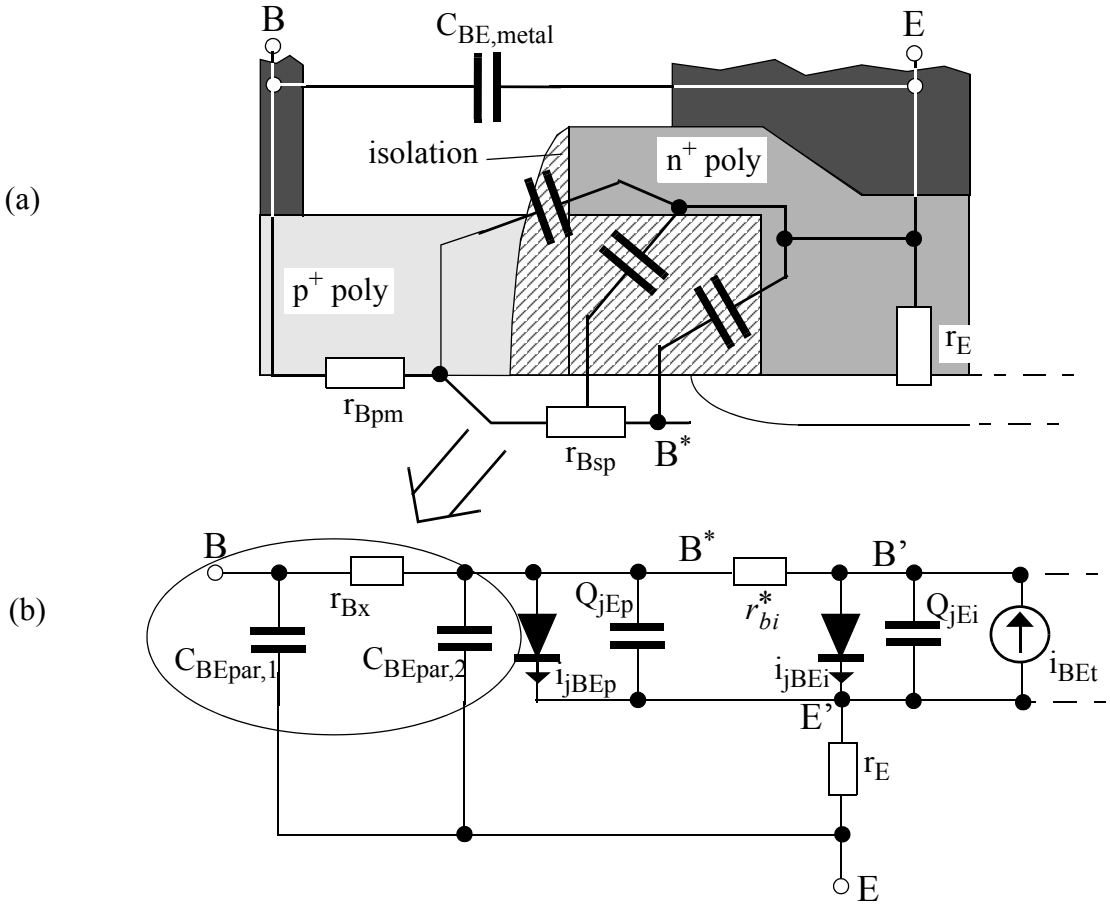

Fig. 2.8.0/1: External and internal base-emitter region: (a) schematic cross-section of left half of base-emitter region with physical series resistance and distributed isolation capacitance components; (b) equivalent circuit with lumped isolation charge (and capacitance) partitioning.

2.9 Substrate transistor

The temperature dependence of the transfer current and the CS junction current have been improved. While the junction current has as already been described in chapter 2.3.2, the transfer current is given by

$$I_{TS}(T) = I_{TSS}(T_0)\left(\frac{T}{T_0}\right)^{\zeta_{BCxT}} \exp\left[\frac{V_{gCeff}(0)}{V_T}\left(\frac{T}{T_0}-1\right)\right], \qquad (2.9.0\text{-}1)$$

with the factor ζ_{BCxT} from (2.3.2-9).

The minority storage time (transit time) of the parasitic substrate transistor under forward operation is described as a function of temperature similar to the other transit time components,

$$\tau_{Sf}(T) = \tau_{Sf}(T_0)\left(\frac{T}{T_0}\right)^{(\zeta_{Cx}-1)}, \qquad (2.9.0\text{-}2)$$

with the temperature factor ζ_{Cx} as additional model parameter, that can be determined from the mobility in the external collector region. ζ_{Cx} corresponds to the exponent in the mobility temperature dependence.

Note, that substrate transistor action can generally be avoided by a surrounding collector sinker.

3 Comments on model implementation

3.1 General bug fixes

Below, a number of cases are given in which certain vendor codes contained the same errors although some of those errors had already been fixed for our Version 2.1.

3.1.1 Transit time equation

The formulation of the normalized injection width *w* at high current densities should contain the normalization term

$$1 + \sqrt{1 + a_{hc}}$$

rather than just the factor "2", which has still been existing in the code of some simulators.

3.1.2 Substrate transistor

Equation (2.1.12-3) on page 64 of the version 2.1 manual correctly contained the formulation

$$Q_{dS} = \tau_{Sf} I_{TSf} \,, \tag{3.1.2-1}$$

but codes (incl. the reference) contained $Q_{dS} = \tau_{Sf} I_{TS}$, in which the current "I_{TS}" has to be replaced by "I_{TSf}".

Also, in the transfer current implementation of the parasitic substrate transistor, the following error was found (which is of little practical relevance though) in DEVICE and some commercial codes: one of the controlling node potentials, **V_BxCi,** should be changed to **V_BpCi**.

3.2 Limiting schemes

In order to avoid numerical overflow, limiting schemes for exponential dependences on node potentials need to be implemented. This proved to be essential for obtaining reliable convergence with the Verilog-A code [11]. In addition, as suggested by [12], the temperature increase resulting from self-heating should be limited to avoid thermal and, hence, numerical instability. Ideally, this type of stability measure should be flagged to the simulator user.

The question to be decided yet, is whether the limiting function(s) should be included within the model to make the model formulation simulator-independent or whether - as adequate alternative - simulator vendors are able to agree on a unified limiting function. The first option will result in

more code related burden on the model developers' side. The second option should be possible to realize using model compilers.

Note, that proper voltage limiting enhances convergence but does not change the final result once convergence occurs; i.e. the final solution does not depend on the type of limiting.

3.3 Recommendations

3.3.1 Self-heating flag

For commercial simulators and model use, it is recommended to *add a flag* (FLSH) for turning on or off self-heating in a given model parameter set that includes non-zero values for R_{th} (RTH) and C_{th} (CTH). Presently, R_{th} itself is used as a flag requiring a change in the model library. A separate flag would be more user friendly and preserve the values in the model card which are lost when the effect is turned off.

The power dissipation is generally caused by all dissipative elements in the equivalent circuit (i.e. excluding any energy storage elements). If *FLSH* = 2, the power in the model is calculated including all the relevant elements in the equivalent circuit as follows,

$$P = I_T V_{C'E'} + \sum I_{jd} V_{diode} + I_{AVL}(V_{DCi} - V_{B'C'}) + \sum \frac{\Delta V_n^2}{r_n} \quad , \tag{3.3.1-1}$$

with d={*BEi,BCi,BEp,BCx,SC*}, V_{diode} as respective diode voltage, r_n as (non-zero) series resistance (n={*Bi,Bx,E,Cx*}) and ΔV_n as the corresponding voltage drop across those resistances.

However, since not only the accuracy of the single-pole network and, in particular, of the determination (and geometry scaling) of R_{th} and C_{th} are fairly limited, but also the consideration of *all* dissipative elements generates elaborate expressions for the derivatives in the Jacobian, only the most relevant dissipative elements are included in the power calculation for *FLSH* = 1:

$$P = I_T V_{C'E'} + I_{AVL}(V_{DCi} - V_{B'C'}) \tag{3.3.1-2}$$

The purpose of this measure is to reduce the computational effort without sacrificing convergence.

3.3.2 Vertical NQS effects

For commercial simulators and model use, it is recommended to *add a flag* (FLNQS) for allowing to turn on or off NQS effects in a given model parameter set, that included non-zero values for α_{IT} (ALIT) and α_{Qf} (ALQF). Presently, α_{IT} and α_{Qf} are used directly as flags, requiring changes in the model library. A separate flag would obviate these changes and also preserve the values in the model card which are lost when the effect is turned off.

The modeling of NQS effects and their implementation in circuit simulators seems to be still under discussion. First of all, it is fairly clear that both current and charge show NQS effects and have to be taken into account in compact model in order to provide the correct phase shift for transconductance and current gain for all types of circuit design. For instance, a simple transcapacitance in the B'C' branch is not only insufficient, but also produces an incorrect increase of the magnitude of the transconductance with frequency.

Secondly, there are occasionally suspicions that a particular implementation of NQS effects causes convergence problems. In one case that was reported, long simulation times occurred for a ring-oscillator with nonzero values for both NQS delay times in the HICUM parameter set. As it turned out, the transistors were driven far into the high-current region, and the model produced the correct results compared to simulations with other models or the NQS delay turned off. Regarding the (conventional "Weil") approach employed in HICUM for implementing NQS effects in time domain, the following quote from a company representative might be of interest:

"*In our SGP model, we do use the Weil approach for excess phase. We have run huge transient simulations (>100k bipolars) without any problems which could be associated with the Weil approach. My guess would be that any problems people report are likely due to the simulator implementation.*"

Note that the "Weil" formulation in the original paper was for an equidistant time step and, thus needs to be extended to non-equidistant time steps. The latter can be found in the HICUM code along with the appropriate (cross-)derivatives.

3.3.3 Noise

In the implementation, the thermal resistance should not assigned any noise mechanism.

In order to improve the agreement between model and measured noise parameters for advanced SiGe and III-V process technologies, it is recommended to include the correlation between base and collector noise. In the literature, so far a delay term

$$c = \exp(j\omega\tau_n) - 1 \tag{3.3.3-1}$$

has been favored as correlation factor, with $\tau_n = \tau_{Bf}/3$ as delay time for a diffusion transistor. For a realistic transistor, the general equation for the vertical NQS delay time of the transconductance, that is already available in HICUM, can be used as a first-order approximation,

$$\tau_n = \tau_m = a_{IT}\tau_f \,. \tag{3.3.3-2}$$

Thus far, the implementation of the correlation factor has turned out to be difficult in Verilog and is still under investigation in order to provide code for generating reference noise data.

Investigations of flicker noise in polysilicon-emitter bipolar transistors seem to indicate that the flicker noise is generated by traps at the polysilicon to monosilicon interface. This corresponds to a strong correlation between the bottom and perimeter component, which is simply modelled as

$$\boxed{\overline{I_{BE}^2} = k_F \left(I_{jBEi} + I_{jBEp}\right)^{a_F} \frac{\Delta f}{f}} \,. \tag{3.3.3-3}$$

According to the version 2.1 documentation the above noise contribution is allocated to the internal base node. However, some simulators seem to have the noise connected to the perimeter base node. For flexibility and backward compatibility, a flag is introduced into the present version to allocate the correlated flicker noise to either the internal base node (*CFBE* = -1) or the perimeter base node (*CFBE* = -2). The default value is -1 for compatibility with version 2.1. The value range [0,1] is reserved for a correlation factor in a possible future implementation.

4 Comments on model release

4.1 Code

Reference code of HICUM Version 2.2 is being made available in Verilog-A. In addition, the updated model version will be available in SPICE3F code [1] (please contact Prof. Jean-Claude Perraud at perraud@ensicaen.ismra.f). Presently, there is no plan for releasing of our own simulator DEVICE [2] to *general* users; however, DEVICE keeps being available to our direct cooperation partners. However, the HICUM v2.2 related *code* of DEVICE will be generally available, since it contains detailed analytical derivatives compared to version 2.1. Using a Verilog model compiler, C-code can be provided as well.

Depending on the future development and availability of model compilers, it is possible that future releases for HICUM can be provided directly as code for specific circuit simulators (i.e. those ones for which the compilers are setup to generate code). Such releases can possibly include model features that are special to the process technologies of cooperation partners for preliminary testing before a release in the standard version.

The code of the new version can be obtained from the following web-site:

http://www.iee.et.tu-dresden.de/iee/eb/eb_homee.html

4.2 Model parameters

The parameters MCF, IS (as alternative to c10), HJEI, HJCI, HFE, HFC, ZETACX have already been available in the reference code of Version 2.1 (some of them even in Version 2.0), but have still not been existing in some commercial simulators. Table 4.2.0/1 summarizes the new model parameters. Note, that the parameters of the temperature dependent bandgap voltage in (2.1.0-1) are not considered as HICUM model parameters since they only need to be changed if different materials than Si are simulated. Ranges of the parameter values are also given, with a bracket (parenthesis) indicating that an endpoint is included (excluded). Few of the parameters (e.g. some flags) take only one of the two or three possible values and the corresponding values are given as *x*/*y* or *x/y/z*, where the parameter takes either of the values given. An empty ‘range’ column indicates that the particular parameter can take any value.

The parameter ALB has to be kept as a parameter for backward compatibility reasons.

name	description	default	range	test	unit	M
ZETACT	exponent coefficient in transfer current temperature dependence	3		3.5	-	-
VGE	effective emitter bandgap voltage V_{gEeff}	VGB	(0:10]	1.07	V	-
ZETABET	exponent coefficient in BE junction current temperature dependence	3.5		4	-	-
VGC	eff. collector bandgap voltage V_{gCeff}	VGB	(0:10]	1.14	V	-
VGS	eff. substrate bandgap voltage V_{gSeff}	VGB	(0:10]	1.17	V	-
TBHREC	base current recombination time constant at the BC barrier for high forward injection (default is v2.1 compatible)	0 (≡ ∞)	[0:inf)	250	ps	-
TUNODE	flag for specifying the base terminal connection of the tunnelling current source: (default v2.1 compatible)	1=perimeter node	[0/1]	0	-	-
CBEPAR	total parasitic BE capacitance (spacer and metal component)	0.0	[0:inf)	0.6E-15	F	M
FBEPAR	partitioning factor of parasitic BE capacitance (default is v2.1 compatible)	1.0	[0:1]	0.5	-	-
FLSH	flag for turning on (1=main currents, 2=all currents) or off (0) self-heating effects	0	0/1/2	1	-	-
FLNQS	flag for turning on (1) or off (0) vertical NQS effects	0	0/1	1	-	-
F1VG	coefficient K_1 in T dependent bandgap equation	$-1.02377E^{-4}$		=	V/K	-
F2VG	coefficient K_2 in T dependent bandgap equation	$4.3215E^{-4}$		=	V/K	-
FLCOMP	flag to ensure compatibility with the previous model version	0	[0:inf)	1	-	-
CFBE	flag for determining where to tag the flicker noise source	-1	-2/-1	-2	-	-
ALB	Relative TC of forward current gain	0		6E-3		

Table 4.2.0/1: List of new model parameters and their meaning. The last column, "factor", specifies the multiplication ("M") factor for parallel devices. Note, that the flags and bandgap voltage parameters in the last two rows are not considered as HICUM model parameters.

Table 4.2.0/2 contains a reference list of those parameters the names of which have been changed in order to make the parameter name consistent or better recognizable. The table also contains parameters that have been deleted. For instance, the parameter KRBI, which was supposed to make the h.f. noise modeling of the internal base resistance more flexible due to uncertain device physics, has been being dropped in Version 2.2. Also, the parameter ALB (relative TC of current gain) will be phased out. For compatibility reasons though, the emitter bandgap voltage can be calculated from ALB if the latter has been specified in a parameter set rather than VGE:

$$V_{gEeff}(0) = V_{gBeff}(0) - (\zeta_{CT} - \zeta_{BET} - \alpha_{Bf} T_0) V_{T0} \ . \qquad (4.2.0\text{-}1)$$

no	old name	new name	(new) meaning
	aljei	ajei	ratio of max to zero-bias internal BE depletion cap
	aljep	ajep	ratio of max to zero-bias perimeter BE depletion cap
	CCOX	CBCPAR	total parasitic BC capacitance (trench and metal component)
	FBC	FBCPAR	partitioning factor of total BC capacitance
	CEOX	deleted	replaced by total parasitic BE capacitance CBEpar and partitioning factor
	KRBI	deleted	-
	~~ALB~~	~~deleted~~	- not deleted for backward compatibility reasons

Table 4.2.0/2: Reference list of model parameters the name of which has changed or which have been deleted.

5 Frequently asked questions

5.1 HICUM names in simulators

The Table below contains a list of various circuit simulators and the respective command to call HICUM.

simulator name	call
ADS	HICUM
ELDO	Level = 9
HSPICE	Level = 8
SPECTRE	bht
APLAC	HICUM
AnalogOffice	HICUM_L2 (npn) , HICUM_L2_P (pnp)
Silvaco SPICE	Level = 6

Table 5.1.0/1: HICUM model call convention in circuit simulators.

5.2 Minority charge and GICCR charge

There is sometimes confusion about the use of the hole charge terms Q_p and $Q_{p,T}$ in various equations and modes of operation. The term Q_p represents the stored charge in the transistor. This charge has to be used in transient analysis and its derivatives define the capacitances to be used in small-signal analysis.

The term $Q_{p,T}$ consists of a weighted sum of the charge contributions from various transistor regions. According to the GICCR, which is derived directly from the transport equation, this term has to used *only* in the denominator of the transfer current formulation.

5.3 Modeling of transit frequency in III-V HBTs

Compared to Si BJTs and SiGe HBTs, in III-V HBTs the transit time through the BC SCR determines the overall carrier transit time. As a consequence, III-V HBTs exhibit often a drop of the transit frequency f_T with increasing voltage V_{CE} (i.e. reverse biased BC junction) in contrast to Si-based transistors. This is shown schematically in Fig. 5.3.0/1. The result of this effect is also a cross-over of the f_T beyond the peak. However, a similar behavior can be observed in Si-based power transistors. Note, that the fundamental mechanisms determining the drop of f_T with collector current density are still the same in both materials, and are described by the critical current in HICUM. the respective simulation example with HICUM in Fig. 5.3.0/2 demonstrates the model's capability of modeling III-V HBTs.

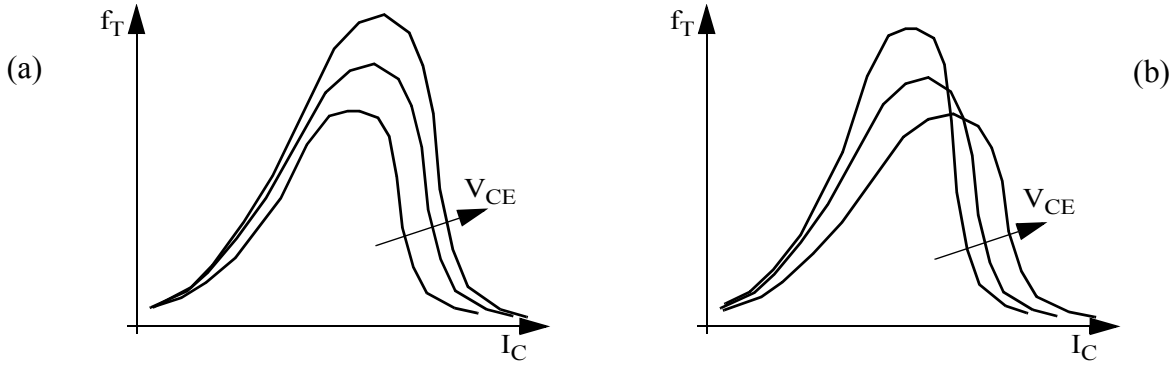

Fig. 5.3.0/1: Schematic shape of f_T characteristics in (a) Si BJTs and SiGe HBTs, (b) III-V HBTs.

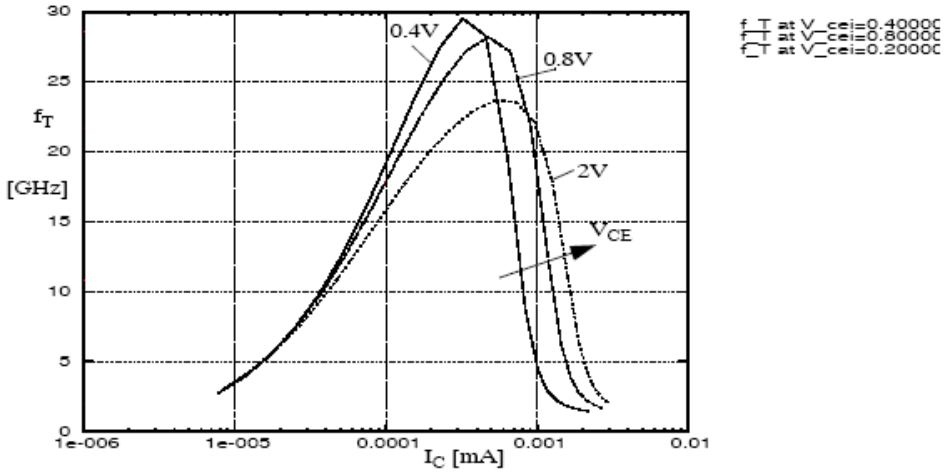

Fig. 5.3.0/2: f_T curves for different V_{CE} values as simulated with HICUM version 2.1; this feature, which enables modeling of III-V HBTs, keeps being available for version 2.2.

5.4 Possible kink in output characteristics

Occasionally, at low voltages $V_{C'E'}$, a kink has been observed in the output characteristics which is has been attributed to a "bad" model parameter combination. Initially, the suspicion was that the limitation formulation used for C_{jCi} at strong forward bias causes τ_{f0}, which is a function of the normalized C_{jCi}, to level off at very low voltages $V_{C'E'}$ and, thus, leads to the observed kink. The voltage $V_{C'E'}$, at which the latter occurs then depends on other model parameters and bias conditions. However, this "effect" would only happen if all other storage times would be turned off which is non-physical. In practice, however, the kink was reported to occur at (very) high current injection.

More detailed investigations revealed that this observation can be reproduced if the inverse transit time τ_r is set to zero or a very small non-physical value. Fig. 5.4.0/1 shows such a case. In Fig. (a), besides the transfer current, which equals the collector current, and displays the kink at a $V_{C'E'}$ of about 0.1V, also the components of the transfer current as well as the hole charge are plotted. It is clearly visible that the kink is linked to the fact that I_{Tf} levels off toward small $V_{C'E'}$, which in turn is caused by the levelling off of the hole charge Q_p. Therefore, in Fig. (b) the charge components are depicted in order to determine the charge that causes Q_p to level off: it is clear that the (forward) minority charge Q_f, which is the dominating component, determines Q_p at low $V_{C'E'}$ values. Q_f levels off toward low $V_{C'E'}$ due to the corresponding smoothing of I_{CK}. At fixed $V_{B'E'}$ the ideal transfer current component I_{Tfi} is also fixed. Therefore, if at two different low voltages $V_{C'E'}$ the critical current I_{CK} is the same, then the forward transit time and charge will also remain the same, leading to a I_{Tf} value that does not depend on $V_{C'E'}$.

Now consider the case for $\tau_r = 0.5$ns as depicted in Fig. 5.4.0/1. The kink has almost disappeared (cf. Fig. (a)), because I_{Tf} decreases toward low $V_{C'E'}$. Although the I_{CK} smoothing has not changed, the additional charge component $Q_r = \tau_r I_{Tr}$, which is proportional $\exp(-V_{C'E'})$, now causes Q_p to increase toward low $V_{C'E'}$ (cf. Fig. (b)). The model employed in HICUM for the inverse charge Q_r is just a simple description of the actual behavior, in which the total minority charge $Q_m = Q_f + Q_r$ certainly increases towards low $V_{C'E'}$ if $V_{B'E'}$is kept constant. Nevertheless, if a more physical approximation of the charge, i.e. $Q_r > 0$ is inserted, the kink disappears. Although the observed kink is undesirable, it is useful to investigate whether a more sophisticated and possibly computationally more expensive minority charge formulation is needed for low voltages $V_{C'E'}$.

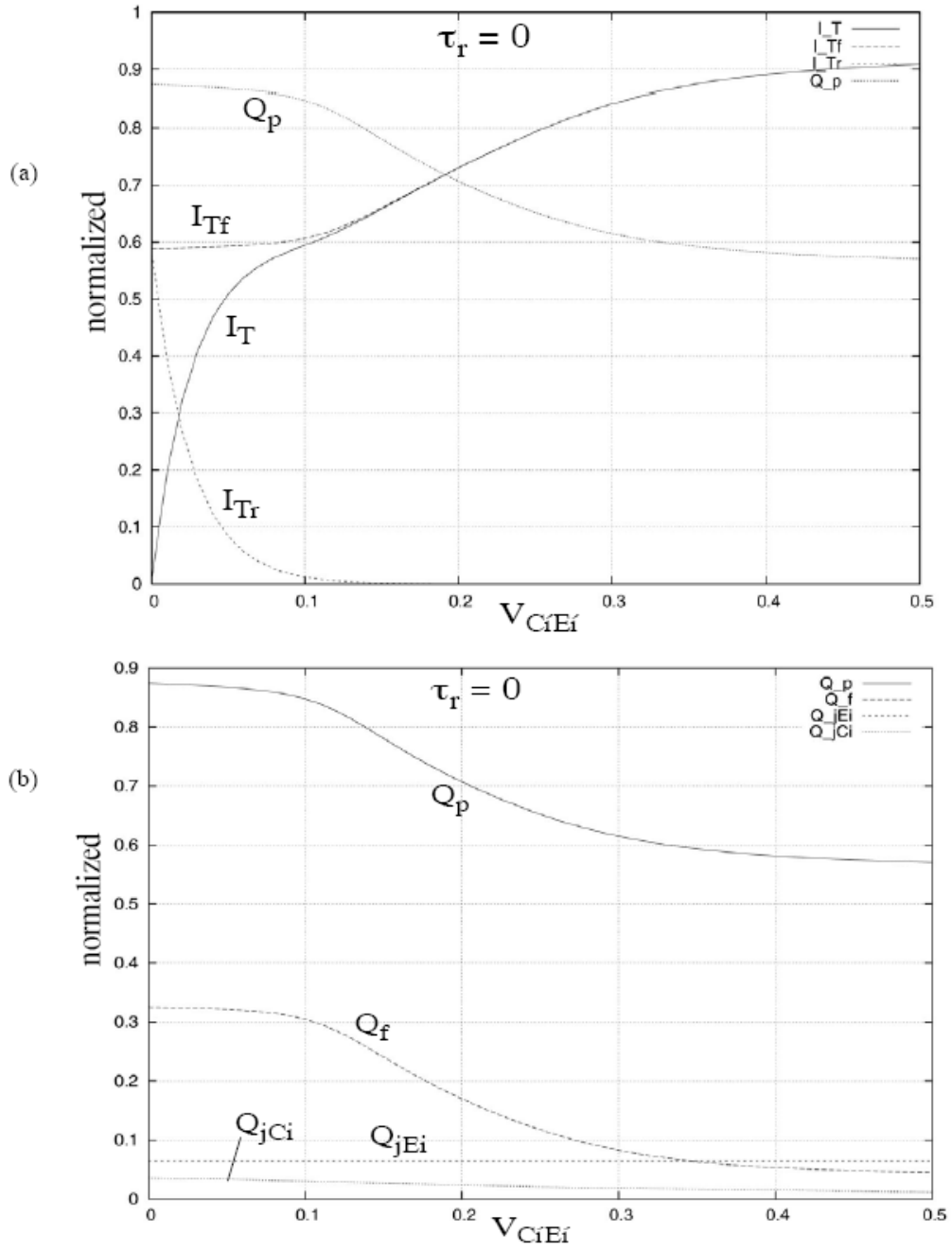

Fig. 5.4.0/1: 1D model results for $\tau_r = 0$: (a) output characteristics with normalized collector and transfer current components; (b) normalized charge components.

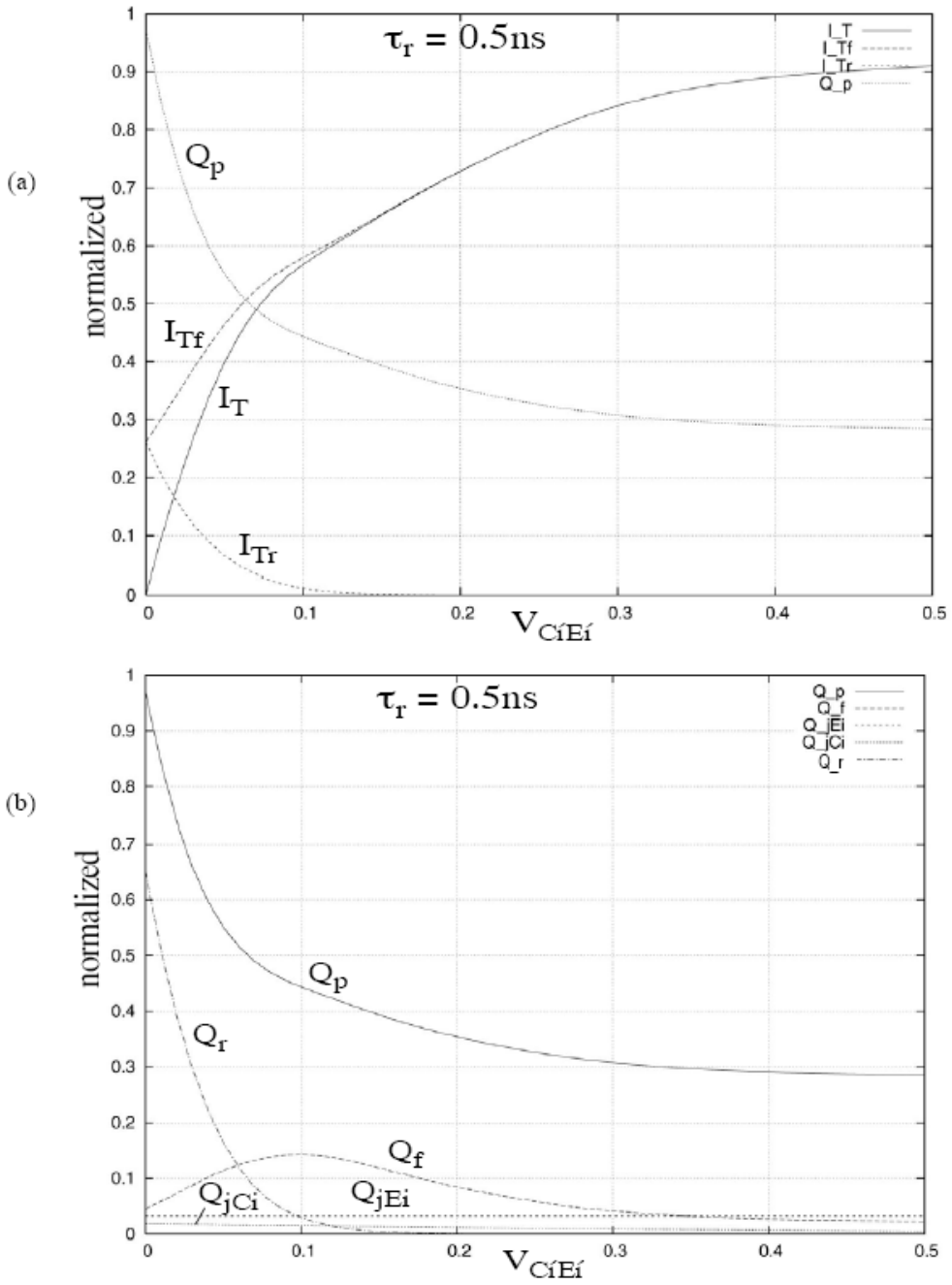

Fig. 5.4.0/2: 1D model results for τ_r = 0.5ns: (a) output characteristics with normalized collector and transfer current components; (b) normalized charge components.

5.5 A note on substrate capacitance and coupling

It has been occasionally requested to offer also a partitioning option for the collector-substrate capacitance. Although this can easily be realized within the HICUM equivalent circuit, it seems to be more flexible to leave it up to the model user to add the appropriate substrate elements in a subcircuit, which not include the CS perimeter capacitance but also the associated substrate coupling network. In fact, depending on the size and type of the substrate-collector transition (e.g., junction, deep trench), a more complicated substrate network may even be required, and the subcircuit will have to be adapted accordingly.

The recommendation for extending the model in a subcircuit by the perimeter components with the most simple network is shown in Fig. 5.5.0/1. The elements within the dash-dotted box are already available in HICUM, while the elements outside of that box would have to be added externally by the user.

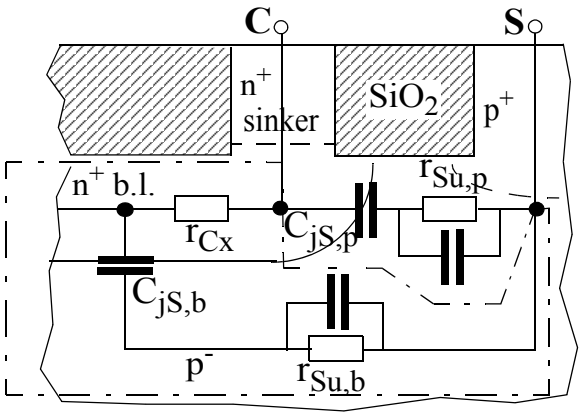

Fig. 5.5.0/1: Recommended extension of the substrate-collector equivalent circuit by a perimeter component.

6 References

[1] For access to SPICE3.F with HICUM, please contact Prof. Jean-Claude Perraud at perraud@ensicaen.ismra.f.

[2] M. Schroter, DEVICE Manual version 1.8, 2004.

[3] S. Lin and C. Salama, "A V_{BE}(T) model with application to bandgap reference design", IEEE Journal of Solid-State Circuits, Vol. 20 , pp. 1283-1285, 1985.

[4] D. Celi, private communications, 2004.

[5] J. Herricht and M. Schroter, "Bandgap reference design considerations and model implications", 3^{d} European HICUM Workshop, Dresden, Germany, June 2003.

[6] HICUM manual version 2.1.

[7] M. Malorny, CEDIC internal report, 2003.

[8] C. McAndrew, private communication, 2003.

[9] C. Jacoboni et al., "A review of some charge transport properties of silicon", Solid-State Electronics, Vol. 20, pp. 77-89, 1977.

[10] M. Schröter, Z. Yan, T.-Y Lee, and W. Shi, "A compact tunnelling current and collector breakdown model", Proc. IEEE Bipolar Circuits and Technology Meeting, Minneapolis, pp. 203-206, 1998.

[11] G. Coram, private communication, 2004.

[12] J.-C. Perraud, private communication, 2004.